Imaging of a patterned and buried molecular layer by coherent acoustic phonon spectroscopy

Mike Hettich, Karl Jacob, Oliver Ristow, Chuan He, Jan Mayer et al.

Citation: Appl. Phys. Lett. **101**, 191606 (2012); doi: 10.1063/1.4767141
View online: http://dx.doi.org/10.1063/1.4767141
View Table of Contents: http://apl.aip.org/resource/1/APPLAB/v101/i19
Published by the American Institute of Physics.

Imaging of a patterned and buried molecular layer by coherent acoustic phonon spectroscopy

Mike Hettich,[1] Karl Jacob,[1] Oliver Ristow,[1] Chuan He,[1] Jan Mayer,[1] Martin Schubert,[1] Vitalyi Gusev,[2] Axel Bruchhausen,[1,a)] and Thomas Dekorsy[1]
[1]*Department of Physics and Center for Applied Photonics, University of Konstanz, Germany*
[2]*IMMM, UMR CNRS 6283, Université du Maine, 72085 Le Mans, France*

(Received 16 July 2012; accepted 29 October 2012; published online 9 November 2012)

A molecular layer of aminopropyltriethoxysilane is patterned with a focused ion beam and subsequently covered by a gold film. The gold-polymer-substrate structures are afterwards imaged by ultrafast coherent acoustic phonon spectroscopy in reflection geometry. We demonstrate that the lateral structure of the covered polymer layer can be detected via the damping time of the vibrational mode of the gold film. Furthermore, we utilize Brillouin oscillations originating from the silicon substrate to map the structures and to estimate the molecular layer thickness. © *2012 American Institute of Physics*. [http://dx.doi.org/10.1063/1.4767141]

Ultrathin molecular layers have developed into an important ingredient in nanotechnology. Many applications use self-assembled monolayers (SAMs) as adhesion layers for the controlled deposition of nanoparticles[1] or DNA.[2] SAMs also play a central role in the fabrication of devices based on molecular electronics, where they are deposited on substrates and coated with metal electrodes to study their electrical transport behaviour.[3,4] Furthermore, patterning of these organic layers is an important step towards chemical addressability of surfaces.[5] Especially for embedded and patterned organic layers, methods are needed which allow for a non-invasive characterization. Coherent acoustic phonon spectroscopy is a versatile tool to image subsurface structures[6–9] and buried ion implanted surfaces.[10] Several investigations have already been carried out on the elastic properties of ultrathin polymer films with this method.[11–19] In our study, we image an embedded and patterned self-assembled organic layer sandwiched between a gold film and a silicon substrate by the damping time of the capping gold layer oscillation. We also utilize the time offset of the so called Brillouin oscillation originating from the silicon substrate to image the structure and to estimate the organic layer thickness. Additionally, we demonstrate that the change in the amplitudes of the Brillouin oscillations in patterned and unpatterned areas enables subsurface mapping.

An ultrathin molecular layer consisting of aminopropyltriethoxysilane (APTES) is prepared. The details regarding the preparation are published elsewhere,[19] and the thickness of the molecular layer in this sample will be discussed later. Atomic force microscopy performed on unpatterend samples reveals a uniform mean thickness of the molecular layers over a range of 5 μm. However, the mean layer thickness varies over larger areas by several nanometers. Friction force microscopy confirms that the molecular layers are closed on a 5 μm scale. Subsequent patterning of the molecular layer is achieved by a focused ion beam (FIB) with Ga^+ ions at an energy of 5 keV. Figure 1(a) shows a scanning electron image of the obtained pattern as well as a schematic drawing in Fig. 1(b). The dark squares with a side length of 10 μm are areas where the molecules are removed by the FIB. Due to transient charging effects caused by the scanning electron microscope (SEM) during the FIB patterning process, the surrounding areas also exhibit a contrast in the SEM image. The base FIB dose used for each square is 3.26×10^2 Ions/μm^2. We chose a low base-dose in order to prevent damage to the silicon substrate. To ensure removal of the molecules we fabricated several squares, which are patterned 10–1000 times, respectively (denoted as base-dose multiplier). After the patterning process, a gold film with 24 nm thickness is thermally evaporated.

We use a Ti:saphhire laser based asynchronous optical sampling system[20,21] to excite and detect coherent acoustic phonons in the structure under investigation. The measurements are carried out in reflection geometry with spot sizes of 1.5 μm. The pump and probe wavelength are set to 790 nm and 820 nm, respectively, in order to decrease backscattered pump light by a bandpass filter. Transient reflectivity changes (Figs. 2(a) and 2(b)) occur due to the ultrafast heating of the sample[22] and the associated excitation of coherent acoustic phonons.[23] Although the gold film thickness exceeds the optical penetration depth of the pump pulse, hot electron diffusion[24] causes a homogeneous stress

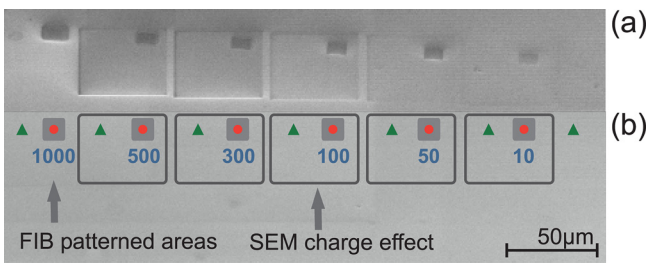

FIG. 1. (a) SEM image of the molecular layer after the FIB patterning process. (b) Schematic drawing, dark squares indicate the areas where the molecules were removed. Larger square areas indicated by black lines are charge effects caused by the SEM. The excitation spots are marked with red dots and green triangles for patterned and unpatterned regions, respectively. Blue numbers indicate the respective FIB base-dose multiplier.

[a)]Also at: Instituto Balseiro & Centro Atómico Bariloche (CNEA), and CONICET, Argentina.

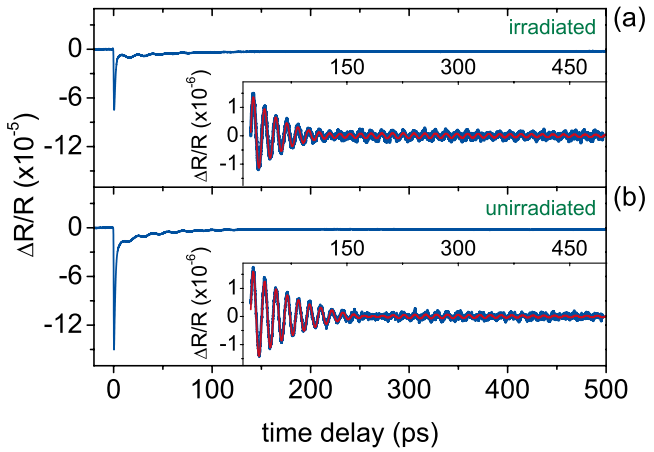

FIG. 2. (a) and (b) show the time domain data for the square with a base-dose multiplier of 300 and the unpatterned region, respectively. The insets show the extracted oscillatory part and the respective fit as thin red line.

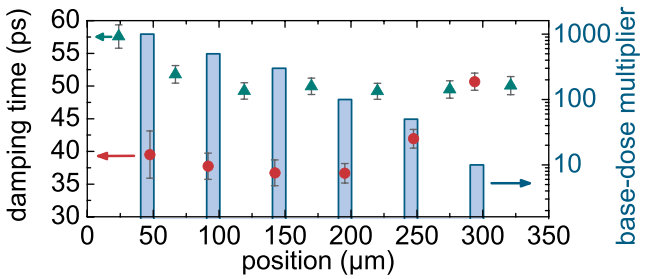

FIG. 3. Damping times plotted versus position. The patterned areas and the respective base-dose multipliers are shown as blue bars. The measured points are marked with red dots and green triangles for patterned and unpatterned regions, respectively. Arrows indicate the respective axis.

distribution. Therefore, the gold film vibrates in its fundamental acoustic mode with a frequency $f = v_{Au}/2d$ determined by the longitudinal sound velocity v_{Au} and the film thickness d.[25] A further, but smaller (i.e., one order of magnitude), oscillatory contribution to the transient reflectivity change arises from a strain pulse propagating in the silicon substrate. The light reflected from the interfaces of the sample interfers with light reflected from the strain pulse. Due to the propagation of the strain pulse, the detected probe light intensity oscillates. These are so called Brillouin oscillations with the frequency $f_{Brillouin} = 2v_{Si}n_{Si}/\lambda$, with the index of refraction n_{Si}, the longitudinal sound velocity v_{Si} and the probe wavelength λ.[26] These oscillations will be discussed later.

The acoustic contributions to the transient reflectivity changes (Figs. 2(a) and 2(b)) are first extracted by a moving average and are fitted with the sum of two exponentially damped sine functions (insets in Figs. 2(a) and 2(b), fits are displayed as thin red lines). From these fits, we obtain the 1/e damping times, frequencies, phases, and amplitudes of both oscillations for varying lateral positions.

We have shown recently that an APTES layer in between a gold film and a silicon substrate influences the damping of coherent acoustic vibrations of the gold film.[19] The damping times can be increased up to factors of ten and three compared to an Au-Si and an Au-SiO_2-Si layer system, respectively. Therefore, a difference in damping times between patterned and unpatterned regions is expected to occur. Figure 1(b) shows the position of the excitation spots on the sample. The resulting damping times are displayed in Fig. 3. We observe a distinct change for the damping times on patterned areas (36 ± 2 ps) when the FIB dose exceeds a base-dose multiplier of 50 compared to unpatterned areas (51 ± 3 ps). For a multiplier of 50, an intermediate state occurs while the square with a base-dose multiplier of 10 exhibits the same damping time as the unpatterned regions. The observed damping times for the patterned regions with a base dose multiplier of 100 and 300 are in good agreement with the calculated value of 35 ps for a perfect Au-SiO_2 interface obtained by the acoustic mismatch model.[10] We attribute the slight increase in damping times for higher base-dose multipliers to the FIB patterning, which causes Ga^+ ion implantation, amorphisation and damaging of the silicon substrate, and the SiO_2 layer.[27,28] Furthermore, Tas *et al.* showed a distinct influence of ion implantation on the damping times in gold films on He^+ doped silicon.[10] Damping times in unpatterned regions vary slightly due to the non-uniform thickness of the molecular layer over a lateral range of 350 μm.

In order to demonstrate the subsurface imaging capabilities of this method, we mapped a part of the square with a base-dose multiplier of 300 with a 7×10 data point grid with 1.7 μm spacing. The obtained damping times are shown in Fig. 4(a) where the damping time is color-coded and plotted versus the position. The areas between the discrete measurement points are interpolated. Red areas correspond to regions where the molecules are still present while they are mostly removed in the blue areas. A line profile indicated by the solid green line is extracted and presented in Fig. 4(d). We obtain a structure width, which agress well to the specified 10 μm in the patterning process.

The time resolved Brillouin scattering can also be employed to image the embedded structure. The time offset of the Brillouin oscillation is proportional to the distance the acoustic pulse propagates until it arrives at the substrate.[29–31] Hence, we compare the Brillouin time shift between areas where the APTES is present to regions where the APTES is removed. The result is shown in Fig. 4(b) as a color-coded plot where we used the lowest time offset as reference value. A comparison to Fig. 4(a) yields a close resemblance, and the areas with a buried molecular layer are well distinguishable by the increased time shift. We use a sound velocity of 2000–2500 m/s (Ref. 12) to calculate the molecular layer thickness. Thus, a mean time shift of 2 ps results in a layer thickness of 4–6 nm. In order to confirm this result, we used transmission electron microscopy (TEM) to measure the organic layer thickness as a reference value. A cross-section of the sample was prepared in the vicinity of the patterned area (i.e., around 10 μm from the scanned square) and was analyzed by high-resolution TEM. The mean molecular layer thickness we obtain by this method is 4.1 ± 0.4 nm. A comparison between the reference measurement and our approach shows a good agreement if we assume the sound velocity to be 2000 m/s. The corresponding APTES layer thicknesses given in nanometers are denoted in Fig. 4(b) in square brackets.

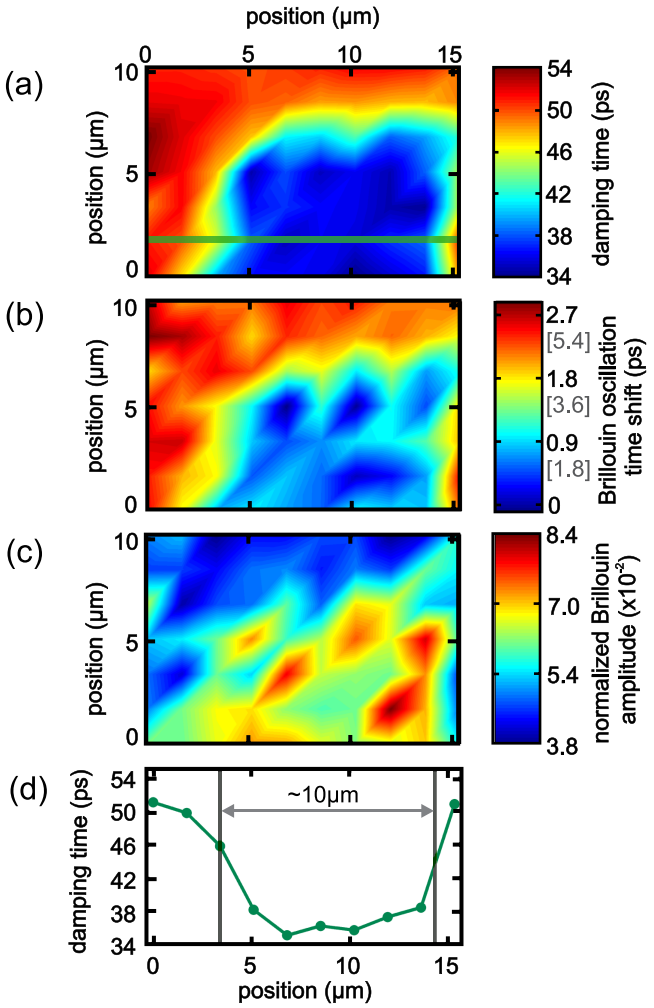

FIG. 4. Color-coded area scans of the square with a base-dose multiplier of 300. (a) Damping time with blue regions corresponding to areas where the molecules are removed. (b) Time offset shift of the Brillouin oscillation. Numbers in square brackets denote corresponding APTES layer thicknesses for a sound velocity of 2000 m/s in nanometers. (c) Brillouin amplitude normalized to the gold film amplitude. (d) Line profile of the solid green line in (a).

We want to mention that due to the FIB patterning, a doped silicon layer may be formed in the irradiated area. Due to the dependence of the Brillouin oscillation time offset on changes in optical properties of the layer system,[32] this would lead to a time shift of 0.6 ps, when we estimate the doped silicon layer thickness with the SRIM program (Ref. 33) to be around 5nm. However, due to the low ion doses used, we expect the change in the optical properties of the doped silicon layer to be negligible.

A further contrast mechanism which stems from the Brillouin oscillation is the decrease in the Brillouin amplitude in areas where a molecular layer is present. Two effects contribute to this decrease. First, the strain pulse amplitude changes due to a change in the acoustic reflection coefficient caused by the APTES layer. This change is evident by the increase in damping times of the gold film oscillation in APTES covered regions. Furthermore, the acoustic pulse may be attenuated while propagating through the molecular layer. Due to the dependence of the Brillouin oscillation on the acoustic pulse amplitude,[34] the decrease in the strain amplitude also gives rise to a decrease in the Brillouin amplitude. The Brillouin amplitude normalized to the gold film amplitude is shown in Fig. 4(c). A comparison to Figure 4(a) shows a decreased image quality but the embedded structure is still visible.

In conclusion, we used coherent acoustic phonon spectroscopy to image a patterned organic layer consisting of aminopropyltriethoxysilane, which is buried under a 24 nm thick gold film. The imaged $10 \times 10\,\mu m^2$ square was fabricated by focused ion beams, and the lateral step size in the imaging process is 1.7 μm. Besides the damping time of the fundamental acoustic mode of the gold film, we use the time resolved Brillouin scattering originating from the silicon substrate as further image contrast mechanism. The differing time offsets of the Brillouin oscillations in APTES covered, and uncovered areas yield a mean APTES layer thickness of 4 nm if we assume a sound velocity of 2000 m/s. This agrees well to the reference measurement conducted by transmission electron microscopy performed on a sample cross-section. The buried structure can also be imaged by the increased Brillouin oscillation amplitude in areas where the molecule is removed. A comparison between these three methods yields the best image quality for the imaging by the damping time. However, the Brillouin time offset allows to obtain information about the layer thickness. Therefore, both methods can be used complementary. The mapping utilizing the Brillouin amplitude shows a decreased image quality compared to the other two methods.

This approach is not limited to a particular molecule but can be applied to detect and image buried layers of different molecule types, thus making it a powerful tool for various applications in nanotechnology especially for the characterization of devices in molecular electronics and sensing.

This work was supported by the DFG through the SFB 767 (Germany) and by the Ministry of Science, Research, and Arts of Baden-Württemberg (Germany). A. Bruchhausen would like to thank the Alexander von Humboldt Foundation (Bonn, Germany) for financial support.

[1]U. C. Coskun, H. Mebrahtu, P. B. Huang, J. Huang, D. Sebba, A. Biasco, A. Makarovski, A. Lazarides, T. H. LaBean, and G. Finkelstein, Appl. Phys. Lett. **93**, 123101 (2008).
[2]B. Gao, K. Sarveswaran, G. H. Bernstein, and M. Lieberman, Langmuir **26**, 12680 (2010).
[3]C. Kreuter, S. Bächle, E. Scheer, and A. Erbe, New J. Phys. **10**, 075001 (2008).
[4]D. Aswal, S. Lenfant, D. Guerin, J. Yakhmi, and D. Vuillaume, Anal. Chim. Acta **568**, 84 (2006).
[5]N. Herzer, S. Hoeppener, and U. S. Schubert, Chem. Commun. **46**, 5634 (2010).
[6]K.-H. Lin, C.-T. Yu, S.-Z. Sun, H.-P. Chen, C.-C. Pan, J.-I. Chyi, S.-W. Huang, P.-C. Li, and C.-K. Sun, Appl. Phys. Lett. **89**, 043106 (2006).
[7]K.-H. Lin, C.-M. Lai, C.-C. Pan, J.-I. Chyi, J.-W. Shi, S.-Z. Sun, C.-F. Chang, and C.-K. Sun, Nat. Nanotechnol. **2**, 704 (2007).
[8]S. Ramanathan and D. G. Cahill, J. Mater. Res. **21**, 1204 (2006).
[9]A. M. Lomonosov, A. Ayouch, P. Ruello, G. Vaudel, M. R. Baklanov, P. Verdonck, L. Zhao, and V. E. Gusev, ACS Nano **6**, 1410 (2012).
[10]G. Tas, J. J. Loomis, H. J. Maris, A. A. Bailes III, and L. E. Seiberling, Appl. Phys. Lett. **72**, 2235 (1998).
[11]A. V. Akimov, E. S. K. Young, J. S. Sharp, V. Gusev, and A. J. Kent, Appl. Phys. Lett. **99**, 021912 (2011).
[12]B. Bonello, G. Louis, and P. Battioni, Rev. Sci. Instrum. **74**, 889 (2003).
[13]B. Bonello, F. Armand, J.-P. Pradeau, H. Perez, B. Perrin, and G. Louis, J. Appl. Phys. **86**, 4959 (1999).

[14]P. M. Walker, J. S. Sharp, A. V. Akimov, and A. J. Kent, Appl. Phys. Lett. **97**, 073106 (2010).
[15]C. J. Morath and H. J. Maris, Phys. Rev. B **54**, 203 (1996).
[16]Y.-C. Lee, K. C. Bretz, F. W. Wise, and W. Sachse, Appl. Phys. Lett. **69**, 1692 (1996).
[17]L. Rouai, B. Bonello, G. Louis, B. Perrin, and P. Peretti, J. Appl. Phys. **85**, 8155 (1999).
[18]G. Tas, R. J. Stoner, H. J. Maris, G. W. Rubloff, G. S. Oehrlein, and J. M. Halbout, Appl. Phys. Lett. **61**, 1787 (1992).
[19]M. Hettich, A. Bruchhausen, S. Riedel, T. Geldhauser, S. Verleger, D. Issenmann, O. Ristow, R. Chauhan, J. Dual, A. Erbe, E. Scheer, P. Leiderer, and T. Dekorsy, Appl. Phys. Lett. **98**, 261908 (2011).
[20]A. Bartels, R. Cerna, C. Kistner, A. Thoma, F. Hudert, C. Janke, and T. Dekorsy, Rev. Sci. Instrum. **78**, 035107 (2007).
[21]R. Gebs, G. Klatt, C. Janke, T. Dekorsy, and A. Bartels, Opt. Express **18**, 5974 (2010).
[22]J. Demsar and T. Dekorsy, *Optical Techniques for Solid-State Materials Characterization*, edited by A. J. Taylor and R. P. Prasankumar (Francis & Taylor, New York, 2010).
[23]O. B. Wright, Phys. Rev. B **49**, 9985 (1994).
[24]C.-K. Sun, F. Vallée, L. H. Acioli, E. P. Ippen, and J. G. Fujimoto, Phys. Rev. B **50**, 15337 (1994).
[25]T. Pezeril, N. Chigarev, D. Mounier, S. Gougeon, P. Ruello, J.-M. Breteau, P. Picart, and V. Gusev, Eur. Phys. J. Spec. Top. **153**, 207 (2008).
[26]H. N. Lin, R. J. Stoner, H. J. Maris, and J. Tauc, J. Appl. Phys. **69**, 3816 (1991).
[27]P. W. Nebiker, M. Dobeli, R. Muhle, M. Suter, and D. Vetterli, Nucl. Instrum. Methods Phys. Res. B **113**, 205 (1996).
[28]S. Rubanov and P. R. Munroe, J. Microsc. **214**, 213 (2004).
[29]P. Emery and A. Devos, Appl. Phys. Lett. **89**, 191904 (2006).
[30]A. Devos, R. Cote, G. Caruyer, and A. Lefevre, Appl. Phys. Lett. **86**, 211903 (2005).
[31]T. Pezeril, C. Klieber, S. Andrieu, and K. A. Nelson, Phys. Rev. Lett. **102**, 107402 (2009).
[32]F. Hudert, A. Bartels, T. Dekorsy, and K. Kohler, J. Appl. Phys. **104**, 123509 (2008).
[33]J. F. Ziegler and J. P. Biersack, Program SRIM, http://www.srim.org, 2010.
[34]C. Thomsen, H. T. Grahn, H. J. Maris, and J. Tauc, Phys. Rev. B **34**, 4129 (1986).